J. Fluid Mech. (1999), *vol.* 382, *pp.* 367–373. Printed in the United Kingdom

Note on a baroclinic analogue of vorticity defects in shear

By R. M. SAMELSON

College of Oceanic and Atmospheric Sciences, 104 Ocean Admin Bldg,
Oregon State University, Corvallis, OR 97331-5503, USA
e-mail: rsamelson@oce.orst.edu

(Received 27 May 1998 and in revised form 30 October 1998)

An approach developed recently to study the dynamics of vorticity defects in homogeneous shear flow extends naturally to the case of baroclinic, quasi-geostrophic flow. It is shown that an inviscid geostrophic flow with uniform vertical shear may be destabilized by introducing a 'potential vorticity defect', an arbitrarily small but sufficiently sharp and horizontally uniform change in stratification or vertical shear. The linear baroclinic problem is nearly identical to the linear homogeneous problem, with differences arising only from the boundary conditions. The nonlinear baroclinic problem differs substantially from the nonlinear homogeneous problem, as the leading-order baroclinic nonlinearity is the Jacobian of the 'inner' streamfunction and potential vorticity in the horizontal plane aligned with the defect. An example of the linear instability is described.

1. Baroclinic defect equations

Since the seminal work of Charney (1947) and Eady (1949), the quasi-geostrophic theory of baroclinic instability has played a central role in geophysical fluid dynamics. Here, it is noted that the approach used by Balmforth, del-Castillo-Negrete & Young (1997) to study the dynamics of small disturbances to homogeneous two-dimensional shear flows (Gill 1965) may be directly adapted to the study of quasi-geostrophic baroclinic shear flows.

Consider the quasi-gestrophic flow of a continuously stratified fluid on an f-plane, described by the dimensionless quasi-geostrophic potential vorticity equation (Pedlosky 1987)

$$q_t + J(\Psi, q) + J(\psi, Q) + J(\psi, q) = 0, \tag{1.1}$$

where $J(a, b) = a_x b_y - a_y b_x$ is the Jacobian derivative with respect to the horizontal coordinates x and y, and $\Psi = -U(z)y$ and $Q = -[\tilde{S}(z)U'(z)]'y$ are the basic-state streamfunction and potential vorticity, respectively, representing a parallel flow with variable stratification and vertical shear. The dimensionless stratification parameter, $\tilde{S}(z) = f^2L^2/N^2(z)D^2$, is a function of the vertical coordinate z, and a prime denotes differentiation with respect to the argument. L and D are characteristic length and depth scales, and $N(z)$ is the dimensional buoyancy frequency. The total streamfunction and potential vorticity are $\Psi+\psi$ and $Q+q$, respectively, where the disturbance streamfunction $\psi(x, y, z, t)$ and potential vorticity $q(x, y, z, t) = \Delta\psi + (\tilde{S}\psi_z)_z$ may have finite amplitude.

The flows of interest here have $\tilde{S}(z)$ and $U'(z)$ constant except in a small vertical interval. That is, $\tilde{S}(z) = S_0[1 + \varepsilon F_S(z/\varepsilon)]$, $U'(z) = \Gamma\,[1 + \varepsilon F_V(z/\varepsilon)]$, where the 'defect'

profile functions $F_S, F_V \sim 1$ in the inner region $|z| \sim \varepsilon \ll 1$ and $F_S, F_V \to 0$ at least quadratically as $|z|/\varepsilon \to \infty$. As ε approaches zero, the stratification and vorticity defects become vanishingly small, but the defect potential vorticity gradient Q_y remains of order one. In this limit, the rate of change with height of the isopycnal slopes is fixed, not the total change of slope in the defect.

In the limit $\varepsilon \to 0$, a reduced set of equations describes the leading-order dynamics. The derivation closely follows the procedure for the homogeneous problem (Balmforth *et al.* 1997; Gill 1965), and is not repeated here. The reduced equations are

$$Z_\tau + \eta Z_x - F' B_x + J(B, Z) = 0, \tag{1.2}$$

$$\hat{B}(k, l, \tau) = -\tfrac{1}{2} H(k, l) \int_{-\infty}^{\infty} \hat{Z}(k, l, \eta, \tau)\, \mathrm{d}\eta, \tag{1.3}$$

where $F(\eta) = F_S(\eta) + F_V(\eta)$; $\hat{B}$ and B are related by the Fourier transform

$$\hat{B}(k, l, \tau) = \int_{-\infty}^{\infty} \int_{-\infty}^{\infty} B(x, y, \tau)\, \mathrm{e}^{-\mathrm{i}(kx+ly)}\, \mathrm{d}x\, \mathrm{d}y, \tag{1.4}$$

and the function H depends on the boundary conditions as described below; horizontally localized (or periodic) disturbances are assumed. Here $\tau = \varepsilon \Gamma t$ and $\eta = \varepsilon^{-1} z$, and the inner-region streamfunction and potential vorticity have been expanded as $\psi \approx \varepsilon \Gamma [B(x, y, \tau) + \varepsilon \phi(x, y, \eta, \tau)]$ and $q \approx \Gamma S_0 Z$, where $Z = \phi_{\eta\eta}$ and the approximations are the neglect of terms of higher order in ε. The evolution equation (1.2) is a reduced form of (1.1), while (1.3) follows from matching inner ($\eta \sim 1$) and outer ($|z| \sim 1$) solutions as $\eta \to \pm\infty$ and $z \to 0^{\pm}$.

For a given H, (1.2)–(1.4) is a closed system for B and Z. The linear terms in (1.2) are equivalent to those that arise in the homogeneous problem, but the nonlinear terms differ: the Jacobian of B and Z is now in the (x, y)-plane, transverse to η, rather than in the (x, η)-plane. The system (1.2)–(1.4) has the momentum (impulse) integral

$$\frac{\mathrm{d}}{\mathrm{d}\tau} \int_{-\infty}^{\infty} \int_{-\infty}^{\infty} yA\, \mathrm{d}x\, \mathrm{d}y = 0, \tag{1.5}$$

and the energy integral

$$\frac{\mathrm{d}}{\mathrm{d}\tau} \int_{-\infty}^{\infty} \int_{-\infty}^{\infty} \left(y \int_{-\infty}^{\infty} \eta Z\, \mathrm{d}\eta + AB \right) \mathrm{d}x\, \mathrm{d}y = 0, \tag{1.6}$$

where A is the inverse Fourier transform of $\hat{A} = \hat{B}/H$. With the definition $Y = Z - F' y$, (1.2) may be rewritten $Y_\tau + J(B - \eta y, Y) = 0$, so the horizontal domain integral of any function of Y is conserved separately for each η.

The outer dynamics reduce to $\Delta\psi + S_0 \psi_{zz} = 0$. For decay on an unbounded domain ($\psi \to 0$ as $|z| \to \infty$), the outer solutions are $\hat{\psi}^{\pm} = \varepsilon \Gamma \hat{B}\, \exp(\mp \kappa z)$, where $\psi = \psi^+$ in $z > 0$, $\psi = \psi^-$ in $z < 0$, and $\kappa = S_0^{-1/2} (k^2 + l^2)^{1/2}$, so

$$H(k, l) = \kappa^{-1}. \tag{1.7}$$

If instead no-normal-flow conditions are imposed at $z = \pm d$, the flow can support Eady instabilities even if $F = 0$; if the inner time scaling is required to hold also at the boundaries, these conditions reduce to $\psi^{\pm} = \pm d\, \psi_z^{\pm}$ at $z = \pm d$, which removes the Eady instability. Then the outer solutions are $\hat{\psi}^{\pm} = \varepsilon \Gamma \hat{B} \left[\cosh \kappa z \mp (\kappa H)^{-1} \sinh \kappa z \right]$, and

$$H(k, l) = \kappa^{-1} \left(\frac{\sinh \kappa d - \kappa d \cosh \kappa d}{\cosh \kappa d - \kappa d \sinh \kappa d} \right). \tag{1.8}$$

The singularity in (1.8) at κ_s, where $\kappa_s d = \coth \kappa_s d$, must be avoided in order that the asymptotic ordering remain consistent. (A reviewer has suggested that the expansion near κ_s might be handled by asymptotic techniques more like those used for marginally stable modes.)

2. Linear disturbances

The linearized defect equations for small disturbances, $(Z, B) = (\zeta, b)$ with $|(\zeta, b)| \ll 1$, may be obtained from (1.2)–(1.4) by dropping the Jacobian term in (1.2). These differ in mathematical structure from the linear homogeneous shear defect equations only through the form of H and by the retention of the dependence of the disturbance on the transverse coordinate y. For constant N ($F_S = 0$), this similarity reflects the usual mathematical correspondence between the baroclinic and homogeneous shear instability problems. Consequently, the analytical treatment of the homogeneous linear normal mode and initial-value problems presented by Balmforth *et al.* (1997) may be carried over with only slight modifications. The Fourier–Laplace transform analysis of the linear initial-value problem leads to the same elements as in the homogeneous problem: Landau damping, $\mathcal{N}$-poles, and quasi-modes, in addition to the normal modes. Only the normal modes grow indefinitely; the others contribute at most transient growth. Some selected results on normal mode instabilities are summarized here, and the reader is otherwise referred to Balmforth *et al.* (1997) and Gill (1965).

With $(\zeta, b) = (\hat{\zeta_0}(\eta), \hat{b}_0) \exp[\mathrm{i}k(x - c\tau) + \mathrm{i}ly]$, the dispersion relation is

$$\int_{-\infty}^{\infty} \frac{F'(\eta)}{\eta - c} \, \mathrm{d}\eta = -\frac{2}{H(k, l)}. \tag{2.1}$$

If $F'(\eta_n) = O$ at the points η_n, $n = 1, 2, \ldots, M$, then a Nyquist analysis reveals that the total number of unstable normal modes cannot exceed $(M + 1)/2$, just as for the homogeneous shear defects. Necessary and sufficient conditions for instability are that at least one such point η_n exists at which also $F''(\eta_n) \neq 0$ and, for (1.7),

$$\int_{-\infty}^{\infty} \frac{F(\eta) - F(\eta_n)}{(\eta - \eta_n)^2} \, \mathrm{d}\eta < 0, \tag{2.2}$$

while for (1.8),

$$\int_{-\infty}^{\infty} \frac{F(\eta) - F(\eta_n)}{(\eta - \eta_n)^2} \, \mathrm{d}\eta \neq 0. \tag{2.3}$$

The result (2.3) is formal, as the asymptotics break down near κ_s. For (1.7), an F-profile with a single minimum will always be stable and a maximum is necessary for instability, while marginality will be reached first at $\kappa = 0$. For (1.8), a single minimum may evidently also be unstable, since the 'asymptote' $M = -2/H$ traverses the entire real axis, and instability will evidently always arise near κ_s; again, the results for (1.8) must be interpreted with caution, because of the singularity of H at κ_s.

Results are shown below for the single-hump profile function $F(\eta) = F_0/(1+\eta^2)$, for which the integral (2.1) may be evaluated by residue theory. There is then instability (growth rates $\omega_i = kc_i > 0$) when $F_0 > F_c = 2/(\pi H)$ if $H > 0$, and when $F_0 < F_c$ if $H < 0$, but no regular neutral modes when $F_0 < F_c$ if $H > 0$ or when $F_0 > F_c$ if $H < 0$.

For $\kappa d \gg 1$, $H \sim \kappa^{-1}$ for both far-field boundary conditions, and the asymptotic estimate of the short-wave cut-off for the single-hump profile is $\kappa_c = \pi F_0/2$ in both cases. The long-wave limit ($\kappa \to 0$) of H depends on the choice of far-field boundary

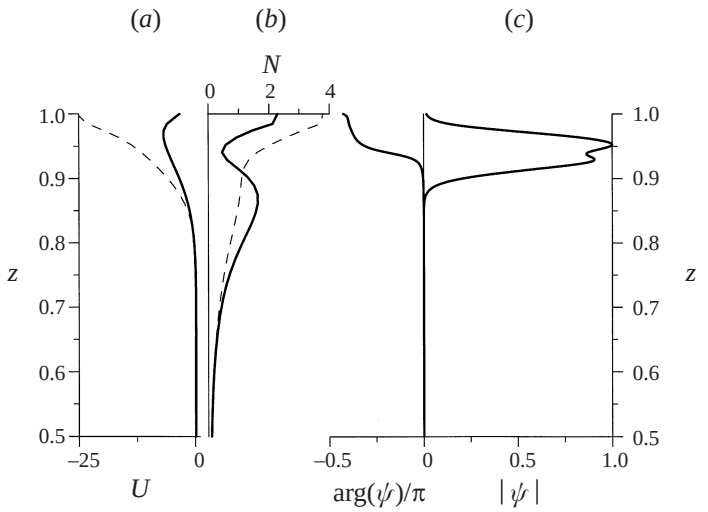

FIGURE 1. Profiles of (*a*) zonal velocity (10^{-3} m s^{-1}) and (*b*) buoyancy frequency N (c.p.h.) versus height above the bottom z (5000 m) from the planetary geostrophic model at the centre of the basin (dark solid line) and at a point directly south of the centre, halfway to the southern boundary (dashed line). (*c*) Amplitude (positive abscissa) and phase divided by π (negative abscissa) for the $k = 40$ mode of the basin-centre profile. Only the upper half of the domain is shown; below mid-depth the variables are essentially uniform.

conditions. In this limit, the growth rates for the single-hump profile are bounded in both cases, but c_i diverges for the unbounded domain, while for (1.8), c_i and ω_i are singular at κ_s.

3. An example

The present analysis was motivated by the appearance of a short-wavelength mode in numerical calculations of the linear quasi-geostrophic instabilities of flow profiles extracted from a planetary geostrophic ocean circulation model. This example is summarized here. The reader is referred to Samelson & Vallis (1997) for a discussion of the planetary geostrophic model.

Two planetary geostrophic flow profiles are shown in figure 1. The first profile was located at the centre of the model basin, and the second directly south of the first and halfway to the southern boundary, but for the present purpose they are taken as independent parallel geostrophic shear flows. The first has a relative minimum in buoyancy frequency N centred at $z = 0.94$ (300 m beneath the surface). The second has N increasingly monotonically with z. In both, the geostrophic zonal velocity U is westward for $z > 0.8$ (within 1000 m of the surface) and negligible for $z < 0.8$. The linear quasi-geostrophic instabilities of these profiles were computed numerically by fitting splines to the profiles N and U, linearizing and discretizing the quasi-geostrophic equations (1.1) with $\psi \propto \exp[\omega_i t + \mathrm{i}(kx - \omega_r t)]$ and linear no-normal-flow boundary conditions at $z = \{0, 1\}$, and solving the resulting matrix eigenvalue problem using standard software routines. The β-effect was included in these computations (i.e. Q was replaced by $Q + \beta y$).

The growth rates ω_i of the fastest growing modes are shown versus zonal wavenumber k in figure 2 for both profiles. For $k < 10$ (wavelengths $\lambda > 30$ km), the characteristics of the growing modes are similar for the two profiles and qualitatively

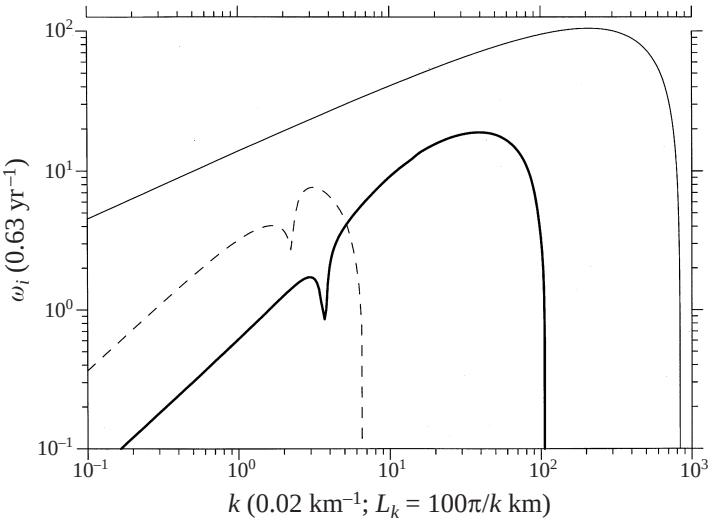

FIGURE 2. Growth rate ω_i (0.63 yr^{-1}) versus zonal wavenumber k (0.02 km^{-1}) for the basin-centre (dark solid line) and south (dashed line) profiles shown in figure 1, and for the defect mode for a single-hump profile on an unbounded domain with $S_0 = 0.1$, $\Gamma = 50$, $\varepsilon = 0.01$, $F_0 = 1686$.

resemble the modes found for uniform shear by Charney (1947), Eady (1949) and Green (1960) and for representative mid-ocean profiles by Gill, Green & Simmons (1974). These modes extend throughout the water column, with structure roughly similar to rest-state baroclinic modes, and largest amplitude near or at the surface.

For the first profile, but not the second, the band of instability extends to $k \approx 100$ ($\lambda \approx 3$ km). The growth rate is maximized near $k = 40$ ($\lambda \approx 8$ km). These short-wavelength modes are confined away from the boundaries, with maximum amplitude and heat flux (proportional to the vertical rate of change of phase) near the buoyancy frequency minimum at $z = 0.94$ (figure 1). In contrast to the Charney (1947), Eady (1949) and Green (1960) modes, they arise from an interior reversal of the potential vorticity gradient, which is dominated by the relative minimum in N embedded in the roughly uniform shear near $z = 0.94$, similar to the term proportional to F_S' in Q_y above. This feature is absent from the second profile, which does not support the short-wavelength instabilities.

For the first profile, the S-profile near the N-minimum may be accurately modelled using the single-hump function, with $S_0 = 0.1$ ($N^2 = 10$), $\varepsilon = 0.01$, and $F_0 = 1686$, while $\Gamma = 50$ approximates the ambient shear. Since the asymptotics assumes $F_0 \approx 1$ and $S \approx S_0$, this is well outside the expected range of validity of the defect approximation. For these parameter values, the defect dispersion relation predicts a maximum growth rate and short-wave cut-off that are an order of magnitude too large, but nonetheless qualitatively resemble the numerical results in the short-wavelength band (figure 2). The defect mode gives an accurate estimate of the thermal potential vorticity structure of the short-wavelength mode near $z = 0.94$, despite the breakdown of the defect asymptotics.

The relation between the defect modes ($F_0 \approx 1$) and the short-wavelength modes ($F_0 \gg 1$) is illustrated in figure 3 for the simpler case of uniform shear in an unbounded domain, using the single-hump profile for the stratification defect. Numerical results were obtained for $S_0 = 0.1$, $\Gamma = 50$, $\varepsilon = 0.02$, and $F_0 = 1, 10, 100, 1000$. For $F_0 = 1$, the defect prediction closely approximates the numerical results. As F_0 increases,

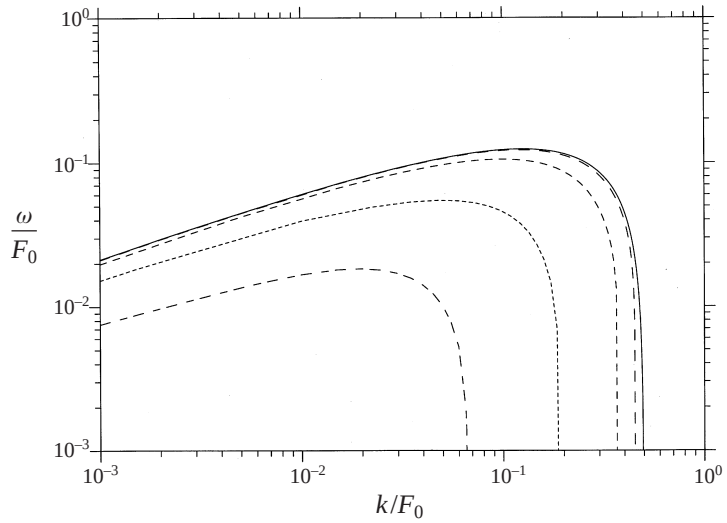

FIGURE 3. Scaled growth rate ω_i/F_0 versus scaled wavenumber k/F_0 for the single-hump profile on an unbounded domain with $S_0 = 0.1$, $\varepsilon = 0.02$. Numerical results for $F_0 = 1, 10, 100, 1000$ are shown (dashed lines), for which the maximum scaled growth rates decrease with increasing F_0. For $F_0 = 1$, the numerical results approach the scaled defect result (solid line), which is independent of F_0.

the growth rates and wavenumbers decrease relative to the defect prediction. For $F_0 = 1000$, the relative difference in growth rates and wavenumbers is similar to that between the defect and short-wavelength modes in figure 2, and the structure of the short-wavelength modes near the growth rate maxima in figures 2 and 3 is similar. This indicates that the short-wavelength instability of the planetary geostrophic flow profile may be understood as the large-F_0 continuation of a bifurcation to instability that is induced by the relative minimum in N as described by the baroclinic defect theory.

4. Discussion

The defect theory yields a linear baroclinic problem that is nearly identical to the linear problem for homogeneous shear flow analysed by Balmforth *et al.* (1997), and offers analogous, analytically accessible examples of baroclinic instabilities that do not depend on the presence of a boundary.

In contrast, the nonlinear baroclinic problem differs substantially from the nonlinear homogeneous problem, as it retains a three-dimensional structure. In the homogeneous shear problem, all the gradients are in the horizontal plane, and one component of the nonlinear term represents the self-advection of disturbance vorticity in a direction transverse to the defect. In the present, baroclinic case, the potential vorticity gradients are horizontal, but the defects arise from sharp vertical gradients, and the nonlinear term represents instead the self-advection of disturbance potential vorticity within the two-dimensional horizontal plane of the defect.

This distinction suggests that the nonlinear development of the baroclinic and homogeneous instabilities will differ in character. In the homogeneous case, it may be anticipated that the transverse advection of disturbance vorticity will lead to roll-up of the defect for nonlinear disturbances. In the baroclinic case, a single linear normal mode is an exact nonlinear solution that will grow indefinitely, since the corresponding

nonlinear terms vanish identically, and for general initial conditions a more turbulent evolution may be anticipated. The quantitative investigation of the nonlinear problem is beyond the scope of the present contribution and is left to future work.

This research was supported by the National Science Foundation, Grant OCE 94-15512. I am grateful for conversations with W. R. Young and D. del-Castillo-Negrete.

REFERENCES

Balmforth, N., del-Castillo-Negrete, D. & Young, W. R. 1997 Dynamics of vorticity defects in shear. *J. Fluid Mech.* **333**, 197–230.

Charney, J. G. 1947 The dynamics of long waves in a baroclinic westerly current. *J. Met.* **4**, 135–163.

Eady, E. T. 1949 Long waves and cyclone waves. *Tellus* **1**, 33–52.

Gill, A. E. 1965 A mechanism for instability of plane Couette flow and of Poiseuille flow in a pipe. *J. Fluid Mech.* **21**, 503–511.

Gill, A. E., Green, J. S. A. & Simmons A. J. 1974 Energy partition in the large-scale ocean circulation and the production of mid-ocean eddies. *Deep-Sea Res.* **21**, 499–528.

Green, J. S. A. 1960 A problem in baroclinic stability. *Q. J. R. Met. Soc.* **86**, 237–251.

Pedlosky, J. 1987 *Geophysical Fluid Dynamics*, 2nd edn. Springer.

Samelson, R. M. & Vallis G. K. 1997 Large-scale circulation with small diapycnal diffusion: the two-thermocline limit. *J. Mar. Res.* **55**, 223–275.